



Subbands in a nanoribbon of topologically insulating MoS₂ in the 1T' phase

Viktor Sverdlov^{a,b,*}, Al-Moatasem Bellah El-Sayed^b, Heribert Seiler^b, Hans Kosina^b, Siegfried Selberherr^b

^a Christian Doppler Laboratory for Nonvolatile Magnetoresistive Memory and Logic at the Institute for Microelectronics, TU Wien, Gußhausstraße 27-29, A-1040 Wien, Austria

^b Institute for Microelectronics, TU Wien, Gußhausstraße 27-29, A-1040 Wien, Austria

ARTICLE INFO

Handling Editor: Bogdan Cretu

Keywords:

Topological insulators
Topologically protected edge states
Nanoribbons
Subbands
 k - p Hamiltonian
Ballistic conductance

ABSTRACT

Continuous miniaturization has brought the feature size of silicon technology down into the nanometer scale, where performance enhancement cannot easily be achieved by further size reduction. The use of new materials with advanced properties has become mandatory to meet the needs for higher performance at reduced power. Topological insulators possess highly conductive topologically protected edge states which are insensitive to scattering and thus suitable for energy efficient high-speed devices. Here, we evaluate the subband structure in a narrow nanoribbon of 1T' molybdenum disulfide by employing an effective k - p Hamiltonian. Highly conductive topologically protected edge modes whose energies lie within the bulk band gap are investigated on equal footing with traditional electron and hole subbands. Due to the interaction between the edge modes at opposite sides, a small gap in their linear spectrum opens up in a narrow nanoribbon. This gap is shown to sharply increase with the perpendicular out-of-plane electric field, in contrast to the behavior in a wide nanoribbon with negligible edge modes interaction. The gap between the traditional electron and hole subbands also increases with the perpendicular electric field. The increase of both gaps leads to a rapid decrease of the ballistic nanoribbon conductance and current with the electric field, which can be used for designing molybdenum disulfide nanoribbon-based current switches.

1. Introduction

Topological insulators (TIs) belong to a new class of materials characterized by highly conductive edge states which lie in the forbidden band gap of the bulk insulating material. In order to have such states in the gap, the bulk host material must possess an inverted band structure with the valence band edge above the conduction band edge. The existence of states with a gapless linear Dirac-like energy dispersion localized at the edge of a TI could be visualized as a result of restoring the standard band order with the conduction band above the valence band at the interface of the host bulk TI with a normal dielectric (air). The edge states are topologically protected by time-reversal symmetry, which results in electron propagation without backscattering.

Edge states in two-dimensional (2D) TIs propagating without backscattering are attractive for designing highly conductive channels [1]. However, possessing robust conductive channels is only one requirement. To make a good switch it is necessary to efficiently control the

current by suppressing it in the off-state as well as to abruptly change between the on- and off-states. A plausible option to control the current efficiently in a 2D TI is to modulate scattering by moving the Fermi level into and out of the bulk bandgap [2]. If the Fermi level lies in the gap, the electrons propagate through the topologically protected edge without backscattering (on-state). In contrast, the electrons from the edge states can scatter and backscatter strongly through the bulk states, if the Fermi level moves out the bandgap and lies in the bulk conduction band or in the valence band. Scattering suppresses the edge states' current by more than two-orders of magnitude compared to the on-state current, thus paving the way to build an imperfect two-dimensional topological insulator field-effect transistor [2].

Recently it was found that the 1T' phase of MoS₂, a well-known 2D material with high promise for future microelectronic devices [3], is a TI [4]. The inverted band structure predicted by *ab-initio* calculations is well approximated by parabolas, with the conduction and valence bands having masses of $m_{\gamma(x)}^{d(p)}$ and their extrema separated by an inverted gap 2δ

* Corresponding author at: Christian Doppler Laboratory for Nonvolatile Magnetoresistive Memory and Logic at the Institute for Microelectronics, TU Wien, Gußhausstraße 27-29, A-1040 Wien, Austria.

E-mail address: Sverdlov@iue.tuwien.ac.at (V. Sverdlov).

<https://doi.org/10.1016/j.sse.2021.108081>

[4]. Without taking spin–orbit interaction into account, the material is a semimetal. The spin–orbit interaction opens a gap at the intersection of the valence and conduction bands, which appears at a finite value of the momentum k_y along the OY axis. A topologically protected highly conductive state with linear Dirac-like energy dispersion along the k_x momentum axis - parallel to the OX axis - exists within this spin–orbit gap and is located at an edge of the MoS₂ sheet in the 1T' phase [4].

Applying an orthogonal electric field, E_z , along the OZ axis perpendicular to a MoS₂ sheet in the 1T' phase offers a possibility to manipulate the bulk spin–orbit gap. With increasing field, E_z , the gap can be reduced, closed, and reopened again [4]. If the gap between the bulk bands reduces, the energy window, within which the edge modes propagate without backscattering, shrinks. Outside of this energy window, efficient scattering between the edge and bulk modes reduces the current carried by the edge modes. When the gap in the host bulk material is closed, scattering between the edge states and the non-protected electron and hole bulk efficiently suppresses the current through the channel, in complete analogy to the imperfect two-dimensional TI field-effect transistor [2]. With further increase of the electric field, the traditional band order is restored indicating a topological phase transition from a non-trivial to a trivial insulator. The gap opens again, but no edge states in the gap are allowed, and any current due to these states is thus completely absent [5]. The ability to modulate the gap and its nature by applying an external electric field therefore opens an alternative and complementary path to control the current flow with the gate voltage by efficiently eliminating the current carrying topologically protected states in the gap [5].

In order to enhance the on-current carried by the edge states it is beneficial to have many edges by stacking several, preferably narrow nanoribbons to decrease the transistor's footprint. However, it is not clear whether the gap between the bulk bands is going to close with increasing electric field, as quantum confinement results in a wider gap. It is therefore expected that the bulk gap never closes in a nanoribbon; however, the quantitative value of the lowest electron and highest hole bulk-like subbands' separation compared to the spin–orbit interaction induced gap is unknown. As the gap between the normal subbands does not close at any electric field, it is even less clear what is going to happen to the topologically protected edge modes and whether the electric current carried by them can be manipulated by applying a perpendicular electric field.

In this article, we evaluate the subband structure in a narrow nanoribbon of 1T'-MoS₂ TI as a function of the orthogonal electric field by employing an effective $\mathbf{k}\cdot\mathbf{p}$ Hamiltonian [4]. The gap between the non-topological bulk-like subbands never closes, instead increasing with the strength of the electric field. We find that a small gap in the spectrum of edge states opens at $k_x = 0$ and we show that it increases with an applied orthogonal electric field. The gap in the edge states is due to an interaction between the states located at opposite edges of a narrow nanoribbon [6]. As the gap increases with the electric field in a nanoribbon, it leads to a rapid decrease in the edge states' ballistic conductance with increasing electric field, which is potentially suitable for switching. However, this is in contrast with recent findings [7]. We elucidate on the reason of the discrepancy and compute the ballistic conductance due to the edge-like modes for several nanoribbon widths.

2. Method

2.1. Effective Hamiltonian

The inverted band structure of 2D MoS₂ in a 1T' phase is well described by the parabolic dispersion relations

$$E_p(k_x, k_y) = \delta - \frac{\hbar^2 k_y^2}{2m_y^p} - \frac{\hbar^2 k_x^2}{2m_x^p} \quad (1)$$

and

$$E_d(k_x, k_y) = -\delta + \frac{\hbar^2 k_y^2}{2m_y^d} + \frac{\hbar^2 k_x^2}{2m_x^d}, \quad (2)$$

where $\mathbf{k} = (k_x, k_y)$ is the wave vector, $E_p(k_x, k_y)$ and $E_d(k_x, k_y)$ refer to the valence and conduction bands, respectively, and $m_{y(x)}^{d(p)}$ denote the effective masses [4]. The bands intersect at $k_y = \pm k_0$, where

$$k_0 = \sqrt{\frac{4\delta}{\hbar^2} \frac{m_y^d m_y^p}{m_x^d + m_x^p}}. \quad (3)$$

Therefore, without taking spin–orbit interaction into account, the material is a semi-metal provided that the Fermi level crosses the intersection points. The spin–orbit interaction makes the conduction and the valence bands interact with each other, which opens gaps around the intersection points at $k_y = \pm k_0$. The effective Hamiltonian \mathbf{H} is written as [4,5]

$$\mathbf{H} = \begin{pmatrix} E_p(k_x, k_y) & 0 & -\alpha E_z - i\nu_1 \hbar k_x & \nu_2 \hbar k_y \\ 0 & E_p(k_x, k_y) & \nu_2 \hbar k_y & -\alpha E_z - i\nu_1 \hbar k_x \\ i\nu_1 \hbar k_x - \alpha E_z & \nu_2 \hbar k_y & E_d(k_x, k_y) & 0 \\ \nu_2 \hbar k_y & i\nu_1 \hbar k_x - \alpha E_z & 0 & E_d(k_x, k_y) \end{pmatrix} \quad (4)$$

Here $\nu_{1(2)}$ are the velocities defining the strength of the spin–orbit interaction and αE_z describes the additional Rashba splitting between the bands due to the perpendicular electric field E_z [5]. E_z can manipulate and change the nature of the gap close to the degeneracy points at $k_y = \pm k_0$. The parameters [4] are listed in Table 1.

It is convenient to perform a canonical transformation of the Hamiltonian (4)

$$\mathbf{H}'(\mathbf{k}) = \mathbf{A}^{-1} \mathbf{H} \mathbf{A} \quad (5)$$

by means of a unitary matrix \mathbf{A} .

$$\mathbf{A} = \frac{1}{2} \begin{pmatrix} 1 & 1 & 1 & 1 \\ 1 & 1 & -1 & -1 \\ 1 & -1 & 1 & -1 \\ 1 & -1 & -1 & 1 \end{pmatrix} \quad (6)$$

After the unitary transformation, the Hamiltonian \mathbf{H}' is in the block-diagonal form

$$\mathbf{H}' = \begin{pmatrix} \mathbf{H}(\mathbf{k}) & 0 \\ 0 & \mathbf{H}^\dagger(-\mathbf{k}) \end{pmatrix}, \quad (7)$$

where (\mathbf{Z}^\dagger) stands for a conjugate transpose matrix \mathbf{Z} . The possibility to express the Hamiltonian in the form (7) is a consequence of the time-reversal symmetry. To simplify the 2×2 Hamiltonian $\mathbf{H}(\mathbf{k})$, we perform the additional transformation

Table 1

Parameters [4] used in the model. m_e is the electron mass, e is the electron charge, and d is the width in OY direction.

Variable	Value
δ	0.33 eV
ν_1	$3.87 \cdot 10^5$ m/s
ν_2	$0.46 \cdot 10^5$ m/s
m_x^p	$0.5m_e$
m_y^p	$0.16m_e$
m_x^d	$2.48m_e$
m_y^d	$0.37m_e$
α	0.03 e nm
k_0	1.386 nm ⁻¹
d	$40k_0^{-1} = 28.86$ nm

$$\mathbf{H}(\mathbf{k}) = \mathbf{B}^{-1} \mathbf{H} \mathbf{B}, \quad (8)$$

with

$$\mathbf{B} = \frac{1}{\sqrt{2}} \begin{pmatrix} 1 & 1 & 0 & 0 \\ -1 & 1 & 0 & 0 \\ 0 & 0 & 1 & 1 \\ 0 & 0 & -1 & 1 \end{pmatrix} \quad (9)$$

The transformation (8), (9) preserves the block-diagonal structure (7). The upper 2×2 block $\mathbf{H}(\mathbf{k})$ is of the form

$$\mathbf{H}(\mathbf{k}) = \begin{pmatrix} \delta - \frac{\hbar^2 k_y^2}{2m_y^p} - \frac{\hbar^2 k_x^2}{2m_x^p} & \nu_2 \hbar k_y - \alpha E_z + i\nu_1 \hbar k_x \\ \nu_2 \hbar k_y - \alpha E_z - i\nu_1 \hbar k_x & -\delta + \frac{\hbar^2 k_y^2}{2m_y^d} + \frac{\hbar^2 k_x^2}{2m_x^d} \end{pmatrix} \quad (10)$$

If we measure energies in units of $E_0 = 2\delta$ and the wave vectors $\mathbf{k} = (k_x, k_y)$ in units of k_0 , the Hamiltonian (10) can be conveniently written in the dimensionless form

$$\mathbf{H}(\mathbf{k}) = \begin{pmatrix} \frac{1}{2} - k_y^2 \frac{m}{m_y^p} - k_x^2 \frac{m}{m_x^p} & \nu_2 k_y - \alpha E_z + i\nu_1 k_x \\ \nu_2 k_y - \alpha E_z - i\nu_1 k_x & -\frac{1}{2} + k_y^2 \frac{m}{m_y^d} + k_x^2 \frac{m}{m_x^d} \end{pmatrix}, \quad (11)$$

where $m = \frac{m_y^d m_x^p}{m_y^d + m_x^p}$ and $\nu_{1(2)}$ are the dimensionless velocities. The Hamiltonian (11) possesses a similar form to the famous Hamiltonian [8] describing the quantum spin Hall effect in Hg/CdTe heterojunctions. However, the relation between the parameters is different, which results in the inverted band structure with the gap open by the spin-orbit interaction at a finite value of $k_y = \pm k_0$. The energy dispersion obtained from (11) and offset by

$$\Delta E = \frac{1}{2} \frac{m_y^d - m_y^p}{m_y^d + m_y^p} \quad (12)$$

is shown in Fig. 1 for $k_x = 0$. If the off-diagonal terms in (11) are zero, the dispersion curves intersect at $k_y = \pm k_0$ and $E_z = 0$. The spin-orbit interaction described by the off-diagonal terms opens a gap at the intersection of the valence and the conduction bands at $k_y = \pm k_0$, (Fig. 1, solid line).

When an electric field E_z along the OZ axis is applied, the gap at one of the minima reduces, completely closes (Fig. 1, dotted line), and opens

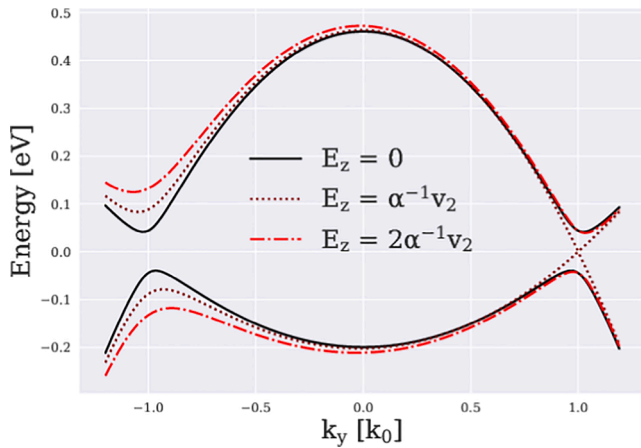


Fig. 1. Bulk energy dispersion in 1T'-MoS₂ two-dimensional material, $k_x = 0$. It displays the gaps at $k_y = k_0$ in the inverted band structure at $E_z = 0$ (solid lines). Increasing the electric field to $E_z = \alpha^{-1}\nu_2$ closes the gap (dotted lines) and reopens it again as a direct gap ($E_z = 2\alpha^{-1}\nu_2$, dot-dashed lines).

again (Fig. 1, dot-dashed line) at large electric fields. The gap at large electric fields becomes direct and the bands are correctly ordered, so no edge states are possible within the bulk gap.

The gap also depends on k_x as shown in Fig. 2. The term which depends linearly on k_x enters in the off-diagonal terms in (11) similar to the term $(\nu_2 k_y - \alpha E_z) \sigma_x$ linear in k_y , where σ_x is the x-Pauli matrix. However, in contrast to the k_y term, the k_x term $-\nu_1 k_x \sigma_y$ enters with σ_y Pauli matrix. As both orthogonal off-diagonal terms define the spin-orbit contribution to the gap Δ , it can be expressed as

$$\Delta = (\nu_1^2 k_x^2 + (\nu_2 k_y - \alpha E_z)^2)^{\frac{1}{2}}. \quad (13)$$

Expression (13) explains the dependence of the gap on k_x seen in Fig. 2. It also explains, why the gap never closes, if the momentum k_x is nonzero.

2.2. Subband calculations

We consider a nanoribbon of width d confined along the OY axis. As the Hamiltonian (7) is block-diagonal, the eigenvalue problem of each block can be solved separately. Since the lower 2×2 block $\mathbf{H}^\dagger(-\mathbf{k})$ of the Hamiltonian (7) is the time-reversal of the upper block $\mathbf{H}(\mathbf{k})$, the corresponding spin-down eigenwave function $\psi_\downarrow(y)$ can be found from the spin-up solution for the upper block in (7) by the time-reversal symmetry transformation $\psi_\downarrow(y) = -i\sigma_y \psi_\uparrow^*(y)$ [6], where σ_y is the Pauli matrix. We therefore only focus on the solutions $\psi_\uparrow(y)$ of the upper 2×2 block Hamiltonian $\mathbf{H}(\mathbf{k})$.

In the transverse direction only quantized values of the momentum $k_y = k_j$ are allowed [9,10]. In addition, it is expected that at $E_z = 0$ two topologically protected edge states localize at opposite edges of the nanoribbon at an energy E within the gap which is opened at $k_y = \pm k_0$ by the spin-orbit interaction.

The subband wave functions $\psi_{k_x}(y)$ in the quantization direction have the general form [9]

$$\psi_{\uparrow k_x}(y) = \sum_{j=1}^4 A_j \begin{pmatrix} a \\ b \end{pmatrix} \exp(ik_j y), \quad (14)$$

where A_j are some expansion coefficients, the wave numbers k_1, \dots, k_4 are the roots of $\varepsilon(k_x, k_j) = E$, where $\varepsilon(k_x, k_j)$ is the bulk dispersion, and the spinor $(a, b)^T$ is an eigenvector of (11) with

$$a = \nu_2 k_j - \alpha E_z + i\nu_1 k_x \quad (15a)$$

$$b = -\frac{1}{2} + k_j^2 \frac{m}{m_y^p} + k_x^2 \frac{m}{m_x^d} + E. \quad (15b)$$

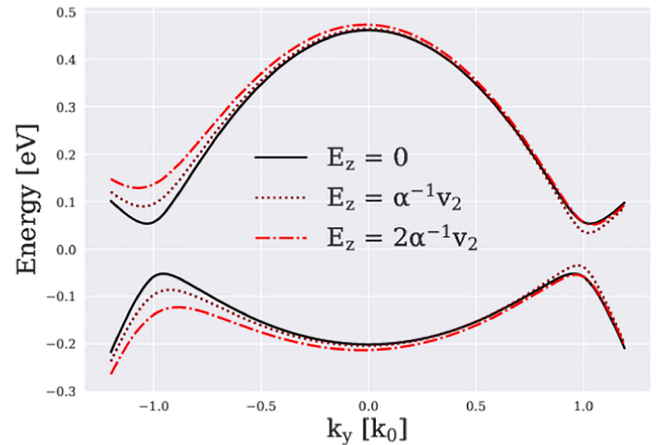


Fig. 2. Bulk energy dispersion in 1T'-MoS₂ two-dimensional material for $k_x = 0.1k_0$ at $E_z = 0$ (solid lines), $E_z = \alpha^{-1}\nu_2$ (dotted lines), and $E_z = 2\alpha^{-1}\nu_2$ (dot-dashed lines).

Setting the wave function at both edges to zero yields the quantization condition

$$\det(\mathbf{M}) = 0, \quad (16)$$

where the matrix $\mathbf{M} = (\mathbf{m}_1 \quad \mathbf{m}_2 \quad \mathbf{m}_3 \quad \mathbf{m}_4)$ is composed of the column vectors \mathbf{m}_j defined as

$$\mathbf{m}_j = \begin{pmatrix} a \\ b \\ a \exp(ik_j d) \\ b \exp(ik_j d) \end{pmatrix} \quad (17)$$

From the condition $\det(\mathbf{E}\mathbf{I} - \mathbf{H}) = 0$ a quartic equation for k_y is obtained:

$$k_y^4 + c_2 k_y^2 + c_1 k_y + c_0 = 0. \quad (18)$$

A simultaneous solution of (16) and (18) is found numerically using the Newton method. We define the unknown vector as $\mathbf{x} = (k_1, k_2, k_3, k_4, E)^T$ and treat k_x as an input parameter. By means of Vieta's formulas a nonlinear equation system of the form $\mathbf{F}(\mathbf{x}) = 0$ can be set up, where the vector-valued function \mathbf{F} is composed of the following components:

$$\begin{aligned} F_1 &= k_1 k_2 k_3 k_4 - c_0 \\ F_2 &= k_1 k_2 k_3 + k_1 k_2 k_4 + k_1 k_3 k_4 + k_2 k_3 k_4 + c_1 \\ F_3 &= k_1 k_2 + k_1 k_3 + k_1 k_4 + k_2 k_3 + k_2 k_4 + k_3 k_4 - c_2 \\ F_4 &= k_1 + k_2 + k_3 + k_4 \\ F_5 &= \det(\mathbf{M}). \end{aligned} \quad (19)$$

In a typical band structure calculation, one chooses an initial point (k_x, E) . To have the Newton iteration converge to an energy close to its initial value and to prevent jumps to some remote subbands, the update vector has to be damped. During the Newton iteration, E is allowed to assume real values only, whereas the k_j are complex.

Fig. 3 displays the behavior of the real part (the imaginary part is zero for $E_z = 0$) of the determinant as a function of energy, for $k_x = 0$. We are interested in the crossings of the curve with the line $E = 0$. The bulk gap due to the spin-orbit interaction occurs at $E \approx \pm 0.06$. The value of the determinant approaches zero from negative values and touches it at a single point. If we now draw a horizontal line at an energy E in Fig. 1 and start moving E from negative values up to positive values, it enters into the gap at $E \approx -0.06$ and leaves the gap at $E \approx 0.06$ for $E_z = 0$ (Fig. 1, solid lines). Therefore, at these energies, the constant energy E

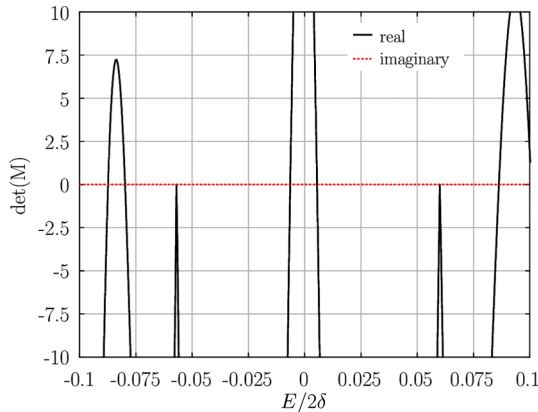


Fig. 3. Real and imaginary parts of $\det(\mathbf{M})$ computed at $k_x = 0$, $E_z = 0$, $d = 40k_0^{-1}$. The bulk gap is seen at $E \approx \pm 0.06$, where the real part touches the line $E = 0$ from below. The subband energies are obtained from $\det(\mathbf{M}) = 0$. Topological edge states are seen in the bulk gap.

horizontal line touches the maximum (minimum) of the dispersion curves. At these points $k_1 = k_2$ and $k_3 = k_4$, which ensures the determinant (16) is zero.

Although (16) is zero at these energies, the roots discussed above must be excluded from the consideration of subbands in a nanoribbon. Indeed, (16) is zero because at least two of the columns (17) are identical due to $k_1 = k_2$ and/or $k_3 = k_4$. In this case the wave function (14) contains only three coefficients A_j which are determined by zero boundary conditions. As the wave function (14) contains two components, and each of the components must be zero at the edges of the nanoribbon, we have an overdetermined system of four linear equations for these three coefficients A_j . The only solution in this case is the trivial one, where the wave function is zero everywhere. Therefore, these roots do not correspond to subbands and must be disregarded. We note here that these solutions were wrongly assigned in [7] to subbands, which resulted in an incorrect interpretation of the results as we discuss later in detail.

All other intersections with the line $\det(\mathbf{M}) = 0$ correspond to subband energies. We clearly observe two roots located in the gap at $E \approx \pm 0.005$. A close inspection shows that the wave numbers k_j corresponding to these two solutions are complex. The wave functions for the spin-up case corresponding to these solutions in the gap are located at an edge of the nanoribbon as shown in Figs. 4 and 5 for $k_x = 0.1k_0$ and $E \approx \pm 0.005$, respectively. The electron ($E \approx 0.005$) wave function shown in Fig. 4 is localized at the left edge of the nanoribbon. Due to time-reversal symmetry, the electron wave function square for the opposite spin orientation (spin down) and for $k_x = -0.1k_0$ coincides with the one shown in Fig. 4. The spin-up wave function is localized at the right edge of the nanoribbon at $k_x = -0.1k_0$. It is a mirror symmetric to the wave function shown in Fig. 4 relative to the center of the nanoribbon.

The wave function for holes ($E \approx -0.005$) in the spin-up case is shown in Fig. 5. It is located at the opposite edge of the wave function for electrons. Following similar arguments, the hole wave functions for the spin-down case and $k_x = \pm 0.1k_0$ can be easily obtained. The wave function for the spin-down case and $k_x = -0.1k_0$ is localized at the left edge, while the wave function for the spin-up case and $k_x = -0.1k_0$ coincides with the one shown in Fig. 5. We note that only the part of the wave function describing the subbands are similar, while the complete wave function includes the plane wave factor describing the propagations in opposite directions along the Ox axis.

In contrast to [6], where only an exponential decay of the edge states was predicted, the wave functions shown in Figs. 4 and 5 display both oscillations and decay. We also note that the period of the electron wave function oscillations is not equal to that of the hole function and is a bit

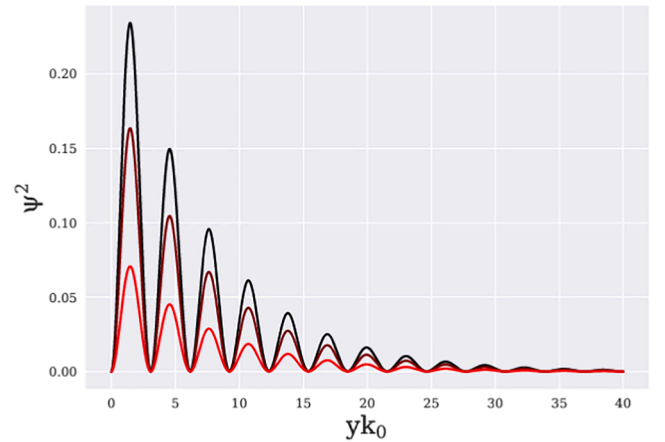


Fig. 4. The wave function squared and its two spinor components, evaluated for the topological edge state at $aE_z = 0.1\nu_2$, $k_x = 0.1k_0$, and $E \approx 0.005$. The wave function shows both oscillation and an exponential decay.

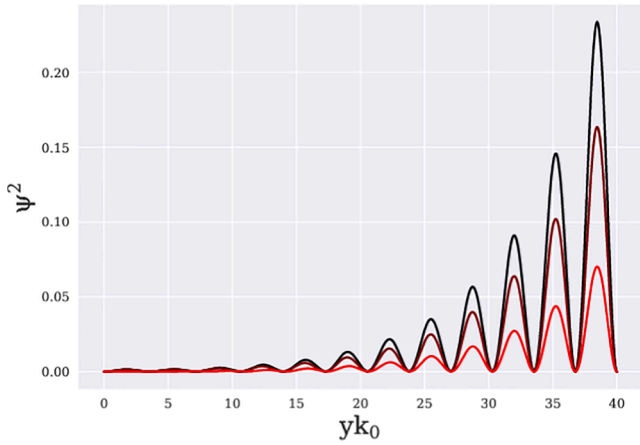


Fig. 5. The wave function squared and its two spinor components, evaluated for the topological edge state at $\alpha E_z = 0.1\nu_2$, $k_x = 0.1k_0$, but $E \approx -0.005$. The wave function is localized at the opposite edge.

shorter. This is because the minima of the hole bands in Fig. 1 are at slightly smaller wave vectors than those of the electron bands. This displacement of the bulk band's minimum from the Gamma-point at $k_y = 0$ is reflected in the oscillations of subband wave functions superimposed on the exponential decay. This displacement is due to different parameters in the otherwise similar Hamiltonian considered in [6], where no oscillations were predicted.

The roots of the determinant for $|E| > 0.06$ correspond to subbands whose k_j are all real. The wave functions are delocalized throughout the width of the nanoribbon. Due to the strong non-parabolicity of the bulk dispersion, the positions of the subband minima and their dispersions can only be found by solving (16) and (18) numerically.

Fig. 6 shows the behavior of the determinant at $\alpha E_z = 0.7\nu_2 k_0$. In this case the gap at $k = k_0$ determined by the extrema of the bulk band structure and the zeroes of (16) at $E \approx \pm 0.02$ is reduced, but not completely closed. The extrema of the bulk band structure at $k = -k_0$ are clearly seen as zeroes of (16) at $E \approx \pm 0.1$.

The edge modes appear close to $E \approx \pm 0.02$. At this particular value of the electric field the edge modes are about to leave the gap and become delocalized as the imaginary parts of two out of four k_j responsible for the localization at the edges become zero. The two solutions at $E \approx \pm 0.075$ have split off from the traditional bulk-like subbands. Their wave functions' behavior is qualitatively different from the bulk subbands' behavior as two out of four of their k_j acquire an imaginary part. This

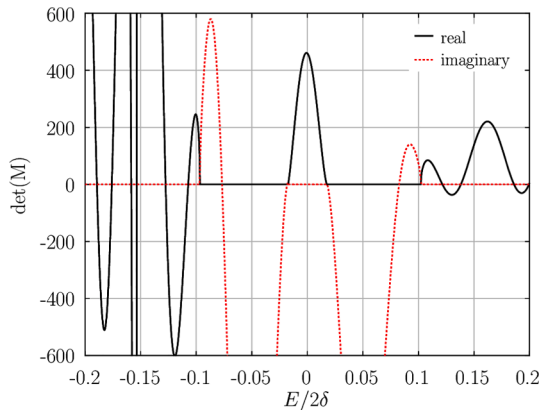


Fig. 6. Real and imaginary parts of $\det(\mathbf{M})$ computed at $k_x = 0$, $\alpha E_z = 0.7\nu_2$, $d = 40k_0^{-1}$. At $E \approx \pm 0.02$ the imaginary part of the two k_j ensuring the localization at the edges approaches zero. New types of roots with imaginary part equals to zero at $E \approx \pm 0.075$ appear.

happens because the gap at $k_y = k_0$ shrinks with increasing E_z , the gap at $k_y = -k_0$ exhibits an opposite trend and becomes wider. Therefore, the lowest traditional subband, whose energy is initially outside of the gap, enters the gap at $k_y = -k_0$ thus forcing the two roots to become complex.

The behavior of the determinant at an even higher electric field $\alpha E_z = 1.4\nu_2 k_0$ is shown in Fig. 7. As the field is larger than the critical field $\alpha E_z = \nu_2 k_0$, at which there is no gap at $k_y = k_0$, the gap seen at $|E| < 0.03$ is now a direct gap. Therefore, no edge states can exist within the direct gap, which is confirmed by the absence of zeroes of the determinant within the direct gap $|E| < 0.03$. There are four subbands lying outside the direct gap at $k_y = k_0$ but still within the gap at $k_y = -k_0$ defined by zeroes of (16) due to the bulk band extrema at $E \approx -0.14$ and $E \approx 0.15$, respectively. While the solutions at $E \approx \pm 0.09$ are split off from the traditional subbands, in complete analogy to the situation in Fig. 6, the subbands at $E \approx \pm 0.05$ originate from the edge states which were continuously pushed outside of the gap at $k_y = -k_0$.

3. Subbands dispersions in nanoribbon

The dispersions of several electron and hole subbands are shown in Fig. 8. The width d of the nanoribbon along the OY axis equals $d = 40k_0^{-1} = 28.86$ nm. The lowest electron/topmost hole subbands possess a linear dispersion. This distinguishes the subbands from traditional subbands in silicon films. The energies of these subbands lie in the bulk band gap (Fig. 1, solid lines). The subbands correspond to the topologically protected edge modes as their wave functions are localized at the edges [11].

A close inspection reveals that a small gap has opened at $k_x = 0$ reflecting the fact that the topological states located at the two opposite edges of the nanoribbon start interacting at $k_x \approx 0$ [6]. At larger k_x the coupling between the edge states becomes insignificant, because the edge states located at opposite edges (Figs. 4 and 5) propagate in opposite directions and do not interact.

Fig. 9 shows the subbands' dispersions at an electric field of $E_z \approx \frac{\nu_2 k_0}{\alpha}$. The gap between the bulk bands would be closed at this field value in an infinitely large system (Fig. 1). However, in contrast to the bulk dispersion, the splitting between the lowest electron and topmost hole subband in a narrow nanoribbon remains finite and actually increases compared to the case without electric field. The splitting becomes even larger at higher electric fields as demonstrated in Fig. 10. As the gap between the lowest electron/topmost hole subband grows with the electric field, their dispersions change from a linear to a quadratic behavior in a broader interval of k_x .

To obtain the higher electron/hole subbands' other roots outside of the bulk gap at $E_z = 0$ must be evaluated. We note that an approximation

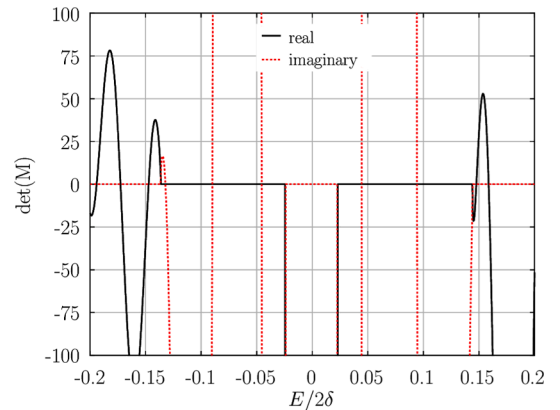


Fig. 7. Real and imaginary parts of $\det(\mathbf{M})$ computed at $k_x = 0$, $\alpha E_z = 1.4\nu_2$, $d = 40k_0^{-1}$. No solution within the direct gap at $|E| < 0.03$ is allowed. Two solutions whose imaginary part are equal to zero at $E \approx \pm 0.05$ and $E \approx \pm 0.08$ are now observed.

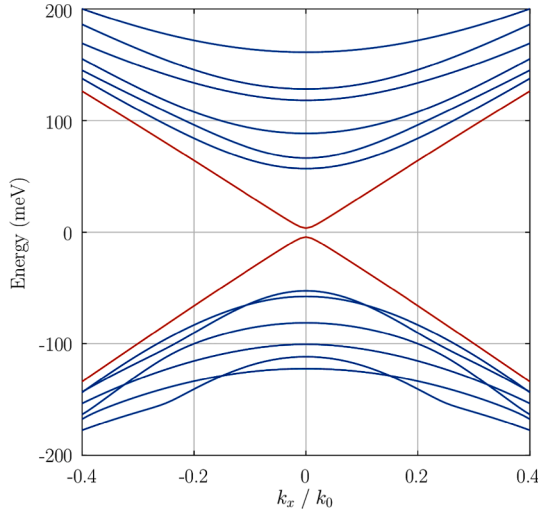


Fig. 8. Subbands in a nanoribbon of the width $d = 40/k_0$, $E_z = 0$. The subband with an almost linear dispersion (in red) corresponding to the topologically protected edge state is clearly seen. A small gap is opened at $k_x = 0$ due to the interaction between the edge modes at opposite edges of the nanoribbon. (For interpretation of the references to colour in this figure legend, the reader is referred to the web version of this article.)

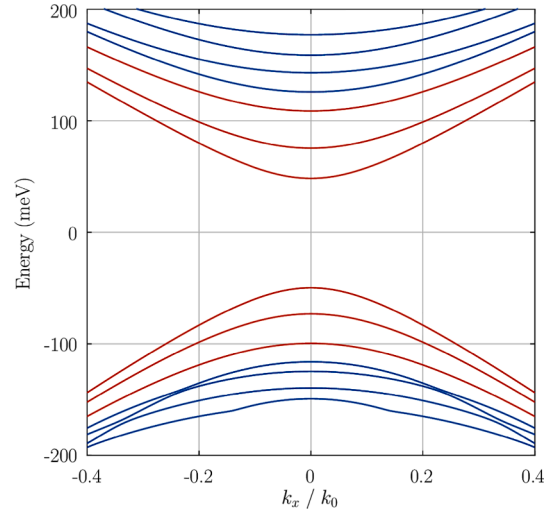


Fig. 10. Subbands in a nanoribbon of the width $d = 40/k_0$ at $\alpha E_z = 2\nu_2 k_0$ when the direct gap is opened again at $k_y = k_0$, see Fig. 1, dot-dashed lines. Now six subbands (in red) at small k_x acquire two real and two complex k_j . (For interpretation of the references to colour in this figure legend, the reader is referred to the web version of this article.)

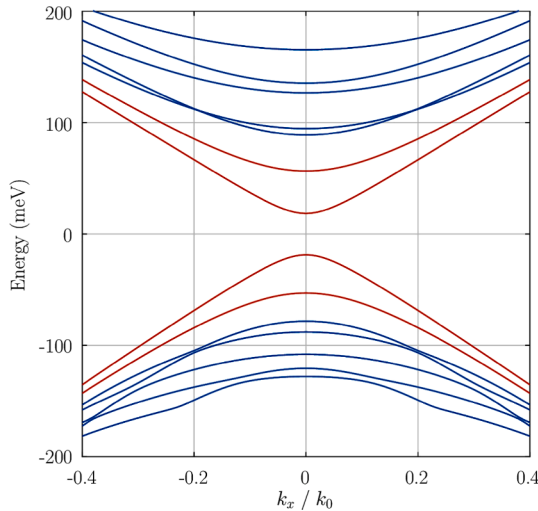


Fig. 9. Subband energies at $\alpha E_z = \nu_2 k_0$, when the gap at $k_y = k_0$ is closed, see Fig. 1, dotted lines. Red lines describe subbands with two real and two complex k_j , while blue subbands have four real k_j real at small k_x . No subbands with linear dispersion are observed. (For interpretation of the references to colour in this figure legend, the reader is referred to the web version of this article.)

of parabolic bands could only be applied to very high energy subbands, as close to the bulk gap the dispersion relation is highly nonparabolic, so (16) must be resolved numerically. Let us define the “bulk” gap in a nanoribbon of a finite width as the gap between the first traditional, non-topological electron and hole subband. Obviously, the gap does not close at $E_z = \frac{\nu_2 k_0}{\alpha}$ (Fig. 9) and keeps increasing for larger electric fields (Fig. 10).

Fig. 11 shows the dependence of the electron (hole) subband minima (maxima) $E_n^{e(h)}$ on the electric field E_z . In agreement with the dispersion relations for a 2D sheet (Fig. 1) the “bulk” gap in a nanoribbon shows signs of a reduction with E_z (Fig. 11), until the field reaches $E_z \approx \frac{0.7\nu_2 k_0}{\alpha}$, after which the trend is inverted and the “bulk” gap starts increasing. This value is lower than the value $E_z = \frac{\nu_2 k_0}{\alpha}$ corresponding to the bands’ inversion in the bulk, Fig. 1, and shown in Fig. 11 by the crossing of the

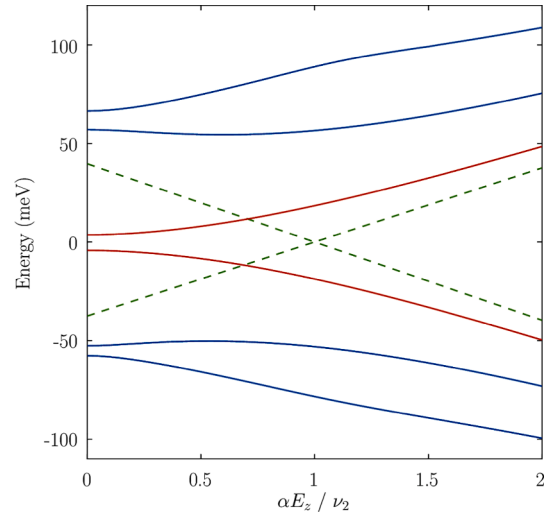


Fig. 11. Dependence of electron ($E > 0$) and hole ($E < 0$) subband minima (maxima) on the electric field E_z for the first three subbands, $dk_0 = 40$. In contrast to the bulk case (shown with dashed lines), the gap never closes and keeps increasing with E_z .

dashed lines. We note that at the value $E_z \approx \frac{0.7\nu_2 k_0}{\alpha}$ of the electric field two of the four values of the wave vectors defining the wave function of edge-localized solutions become real (Fig. 6), so the edge wave function (14) becomes “delocalized” across the width of the nanoribbon.

Let us now compare the dispersions shown in Figs. 9 and 3c from [7]. The striking distinction is the absence of the linear bulk-like dispersion which is attributed to the edge modes in [7]. Although the determinant (16) is zero along this linear dispersion, these solutions are not related to the edge modes. These zeroes of (16) appear at the energies corresponding to the extrema of the bulk dispersion. At the extrema with energy E , the two roots k_j of the equation $\varepsilon(k_x, k_j) = E$ are equal. It immediately causes the determinant (16) to become zero, because the two columns (17) are identical. In the case of $\alpha E_z = \nu_2 k_0$, the bulk dispersion is linear as seen in Fig. 1. Although these solutions give zeroes of (16), they have nothing to do with the subband solutions satisfying (16) because of the boundary conditions, the subband wave function

must satisfy. Therefore, the linear bulk-like modes seen in Fig. 3c of [7] must be disregarded as they do not correspond to the subbands. The subband spectrum is gapped as shown in Fig. 9.

Our conclusion is based on the assumption that the wave function is in the form (14) valid when all four of the roots k_j of the equation $\varepsilon(k_x, k_j) = E$ are different. Although it is not the case at isolated points where the two roots k_j of the equation $\varepsilon(k_x, k_j) = E$ coincide, it does not affect the generality of our result. As we prove in the Appendix, the zero boundary conditions on the wave function can only be satisfied at a very specific, discrete set of nanoribbon widths. The set of widths is different for any k_x momentum. As we show in the Appendix, for a fixed nanoribbon width, the boundary conditions can only be satisfied at isolated k_x points. A continuous solution does not exist and, therefore, no subband with a continuous dispersion corresponding to the degenerate roots k_j .

In order to further demonstrate the fact that the linear dispersion observed in Fig. 3c of [7] does not correspond to any subband, we plot the lowest electron/topmost hole subbands' energy dependence on the electric field for several nanoribbon widths in Fig. 12. The gap between the lowest electron and topmost hole subband increases with the nanoribbons width decreased. The transition, when the confined edge-like states becomes delocalized along the whole width of the nanoribbon, is determined by the intersection of the corresponding dispersions with the dashed lines in Fig. 12 showing the dependence of the bulk bands on E_z . As is seen from Fig. 12, this transition shifts towards lower electric field values for narrow nanoribbons.

At the same time, the minimum and maximum of the bulk bands at $k_y = k_0$, incorrectly attributed in [7] to the edge-like modes and shown in Fig. 12 with green dashed lines, display a linear dependence on the electric field but do not depend on the nanoribbon width. This confirms our claim that these linear solutions due to the extrema of the bulk dispersion must be disregarded for describing the quantized subbands in a nanoribbon.

4. Ballistic conductance

An increase in the energy separation between the electron and hole subbands (Fig. 11) in nanoribbons as a function of a perpendicular electric field is reflected in a rapid decrease of the nanoribbon ballistic conductance [12]. The ballistic conductance is computed as

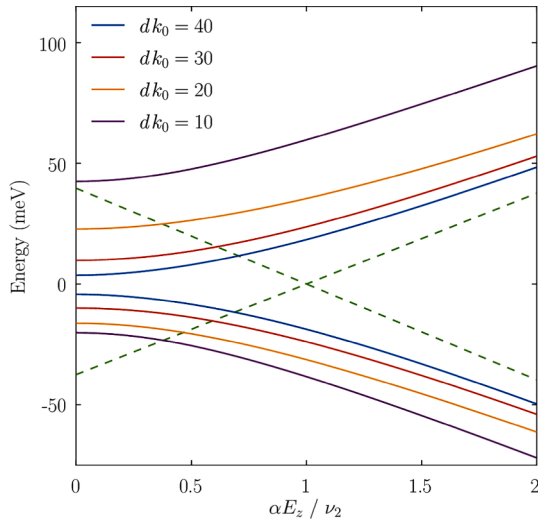


Fig. 12. Dependence of the lowest electron and topmost subbands on the perpendicular electric field in nanoribbons of different widths. The separation gap between the subbands increases with E_z . The dependence of the bulk bands minimum and maximum at $k_y = k_0$ on E_z is shown with dashed lines.

$$G = \frac{2e^2}{h} \sum_i \left[\frac{1}{\exp\left\{\frac{E_i^e - E_F}{k_B T}\right\} + 1} + \frac{1}{\exp\left\{\frac{E_i^h - E_F}{k_B T}\right\} + 1} \right], \quad (20)$$

where T is the temperature and E_F is the Fermi energy. If the Fermi energy is close to the middle of the gap ($E_F \approx 0$), the edge-like subbands dominate the conductance G [12]. The role of the traditional subbands is non-negligible as the two lowest (topmost) electron (hole) bulk-like contribute 30% of the ballistic conductance. However, all contributions to the total conductance G rapidly decrease as a function of E_z . This makes 1T'-MoS₂ promising for switching applications [12].

Let us evaluate the ballistic conductance due to the lowest electron and topmost hole edge-like subband only and compare it with the results of [7] for different nanoribbon widths. As it is seen in Fig. 13, the ballistic conductance decreases with the perpendicular electric field. This is in sharp contrast with [7] where, after an initial decrease, the ballistic conductance starts increasing at higher fields. The increase of the ballistic conductance in [7] is the consequence of the extrema of the bulk dispersion. Although (16) is satisfied, these roots are not due to the subbands and must be disregarded as demonstrated above. Therefore, the ballistic conductance due to the lowest electron/topmost hole subband decreases with increasing electric field E_z .

5. Conclusion

The subband structure in a narrow nanoribbon of 1T' molybdenum disulfide as a function of an out-of-plane electric field is evaluated by employing the effective four-band $\mathbf{k}\cdot\mathbf{p}$ Hamiltonian. It is shown that by an appropriate unitary transformation the Hamiltonian can be recast in a convenient block-diagonal form used to describe topological insulators. In a confined geometry of a nanoribbon the Hamiltonian describes the complete subband structure including topologically protected edge modes. In contrast to the behavior in a wide nanoribbon, where the bulk gap closes at a certain field value and becomes direct at higher values of the electric field, the gap between the traditional lowest electron and highest hole subband never closes and increases with the perpendicular electric field. The increase in the separations between the electron and hole subbands leads to a substantial decrease of their contribution to the total ballistic conductance and current as a function of the perpendicular electric field.

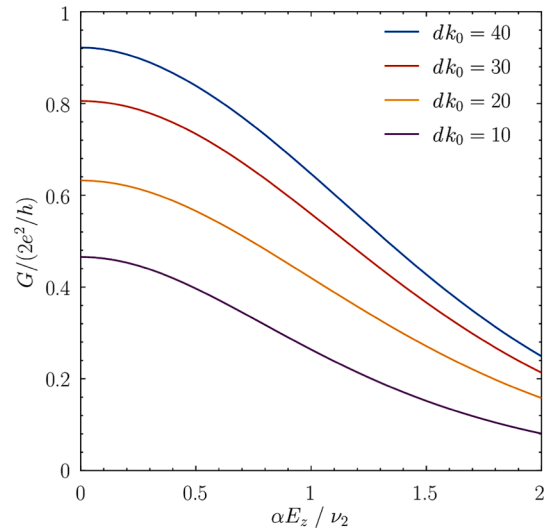


Fig. 13. Ballistic conductance due to the lowest electron-topmost hole subband in a 1T'-MoS₂ nanoribbon of different widths. The ballistic conductance keeps decreasing with E_z increased.

The edge modes' energies lie in the bulk gap. Their dispersion relations are almost linear as a function of the momentum along the nanoribbon and their wave functions are localized at the edges and display damped oscillation. Due to the interaction of the edge modes located at the opposite sides of a narrow nanoribbon, a small gap in their linear dispersion spectrum opens at momenta close to zero. The gap increases rapidly with a perpendicular electric field resulting in a substantial decrease of the contribution due to the edge modes in the ballistic conductance. As the ballistic conductance decreases substantially, varying the electric field is shown to be an attractive option for designing molybdenum disulfide nanoribbon-based current switches.

Declaration of Competing Interest

The authors declare that they have no known competing financial

interests or personal relationships that could have appeared to influence the work reported in this paper.

Acknowledgment

Financial support by the Austrian Federal Ministry for Digital and Economic Affairs, the National Foundation for Research, Technology and Development and the Christian Doppler Research Association is gratefully acknowledged. A.-M.B.E.-S. was supported in part by project No. IN 23/2018 'Atom-to-Circuit modeling technique for exploration of Topological Insulator based ultra-low power electronics' by the Centre for International Cooperation & Mobility (ICM) of the Austrian Agency for International Cooperation in Education and Research (OeAD).

Appendix

In order to find the subbands in a nanoribbon of the widths d along the OY axis we must solve the Schrödinger equation with the Hamiltonian (11) for the wave function $\psi_{\uparrow k_x}(y)$ and energy dispersion $E(k_x)$.

$$(\mathbf{H} - E(k_x) \cdot \mathbf{I})\psi_{\uparrow k_x}(y) = 0 \quad (\text{A1})$$

The wave function must satisfy zero boundary conditions at both edges of the nanoribbon.

$$\psi_{\uparrow k_x}(y=0) = \psi_{\uparrow k_x}(y=d) = 0 \quad (\text{A2})$$

(A1) is a second-order differential equation. To find its general solution as a function of y , we have to determine the k_y roots of the characteristic equation

$$\det(\mathbf{H} - E \cdot \mathbf{I}) = 0 \quad (\text{A3})$$

It is equivalent to finding the k_y roots of the equation

$$\varepsilon(k_x, k_j) = E, \quad (\text{A4})$$

where $\varepsilon(k_x, k_y)$ is the bulk energy dispersion of an infinite sheet and $k_j, j = 1, \dots, 4$ are the four k_y roots of the characteristic Eqs. (A3) and (A4).

If all four roots k_j are different, the wave function is of the form (14). However, when any two of the roots $k_1 = k_2 = k$ are equal, the wave function is of the form

$$\psi_{\uparrow k_x}(y) = (A_1 + A_2 y) \begin{pmatrix} a \\ b \end{pmatrix} \exp(iky) + \sum_{j=3}^4 A_j \begin{pmatrix} a_j \\ b_j \end{pmatrix} \exp(ik_j y), \quad (\text{A5})$$

where the spinor $(a_j, b_j)^T$ is defined by (15) with $k_y = k_j$.

In order to have a nontrivial solution satisfying (A2) the following determinant must be zero:

$$\begin{vmatrix} a & 0 & a_3 & a_4 \\ b & 0 & b_3 & b_4 \\ a \exp(ikd) & a d \exp(ikd) & a_3 \exp(ik_3 d) & a_4 \exp(ik_4 d) \\ b \exp(ikd) & b d \exp(ikd) & b_3 \exp(ik_3 d) & b_4 \exp(ik_4 d) \end{vmatrix} = 0 \quad (\text{A6})$$

By replacing the first column with a linear combination of the first and second column the determinant (A6) reduces to

$$\begin{vmatrix} a & 0 & a_3 & a_4 \\ b & 0 & b_3 & b_4 \\ 0 & a & a_3 \exp(ik_3 d) & a_4 \exp(ik_4 d) \\ 0 & b & b_3 \exp(ik_3 d) & b_4 \exp(ik_4 d) \end{vmatrix} = 0. \quad (\text{A7})$$

From here we obtain:

$$\begin{vmatrix} ba_3 - ab_3 & ba_4 - ab_4 \\ (ba_3 - ab_3) \exp(ik_3 d) & (ba_4 - ab_4) \exp(ik_4 d) \end{vmatrix} = 0 \quad (\text{A8})$$

We introduce

$$c_1 = ba_3 - ab_3, \quad (\text{A9a})$$

$$c_2 = ba_4 - ab_4. \quad (\text{A9b})$$

Because the spinors $(a, b)^T$ and $(a_j, b_j)^T, j = 3, 4$ evaluated at nonequal roots $k_1 = k_2 = k$ and $k_j, c_{1,2}$ in (A9) are always nonzero.

(A8) is rewritten as

$$c_1 c_2 \exp(ik_3 d) = c_1 c_2 \exp(ik_4 d). \quad (\text{A10})$$

It is satisfied only, if

$$\exp(ik_3 d) = \exp(ik_4 d). \quad (\text{A11})$$

If k_3 is different from k_4 , (A11) is equivalent to

$$d_n = \left| \frac{2\pi n}{k_3 - k_4} \right|, \quad n = 1, 2, \dots \quad (\text{A12})$$

Because k_3, k_4 are uniquely defined by the extremum of the energy E of the bulk dispersion $\varepsilon(k_x, k) = E$ at fixed k_x and E_z . (A12) is an equation for d . As d_n depends on k_x , these discrete isolated solutions do not correspond to any subband in a ribbon of the fixed width d and must be disregarded.

If $k_3 = k_4$ which may only happen at $E_z = 0$, $k_3 = -k$, and the wave function has the form

$$\psi_{1k_x}(y) = (A_1 + A_2 y) \begin{pmatrix} a \\ b \end{pmatrix} \exp(iky) + (A_3 + A_4 y) \begin{pmatrix} a_3 \\ b_3 \end{pmatrix} \exp(ik_3 y). \quad (\text{A13})$$

This results in the following determinant:

$$\begin{vmatrix} a & 0 & a_3 & 0 \\ b & 0 & b_3 & 0 \\ 0 & a & 0 & a_3 \\ 0 & b & 0 & b_3 \end{vmatrix} = -(ab_3 - a_3b)^2 \quad (\text{A14})$$

As the spinors $(a, b)^T$ and $(a_3, b_3)^T$ are the eigenfunctions of (11) with different $k_3 = -k$, (A13) can have only accidental isolated roots, see e.g. (15). Therefore, no subband exists with a continuous dispersion corresponding to the degenerate roots k_j .

References

- [1] Kou L, Ma Y, Sun Z, Heine T, Chen C. Two-dimensional topological insulators: progress and prospects. *J Phys Chem Lett* 2017;8(8):1905–19. <https://doi.org/10.1021/acs.jpclett.7b00222>.
- [2] Vandenberghe WG, Fischetti MV. Imperfect two-dimensional topological insulator field-effect transistors. *Nat Commun* 2017;8. <https://doi.org/10.1038/ncomms14184>. 14184.
- [3] Illarionov Yu, Banskchikov AG, Polyushkin DK, Wachter S, Knobloch T, Thesberg M, et al. Ultrathin calcium fluoride insulators for two-dimensional field-effect transistors. *Nat. Electron.* 2019;2:230–5. <https://doi.org/10.1038/s41928-019-0256-8>.
- [4] Qian X, Liu J, Fu L, Li Ju. Quantum spin Hall effect in two-dimensional transition metal dichalcogenides. *Science* 2014;346(6215):1344–7. <https://doi.org/10.1126/science.1256815>.
- [5] Liu L, Guo J. Assessment of performance potential of MoS₂-based topological insulator field-effect transistors. *J Appl Phys* 2015;118. <https://doi.org/10.1063/1.4930930>. 124502.
- [6] Zhou B, Lu H-Z, Chu R-L, Shen S-Q, Niu Q. Finite size effects on helical edge states in a quantum spin-Hall system. *Phys Rev Lett* 2008;101. <https://doi.org/10.1103/PhysRevLett.101.246807>. 246807.
- [7] Das B, Sen D, Mahapatra S. Tuneable quantum spin Hall states in confined 1T' transition metal dichalcogenides. *Sci Rep* 2020;10. <https://doi.org/10.1038/s41598-020-63450-5>. 6670.
- [8] Bernevig BA, Hughes TL, Zhang S-C. Quantum spin Hall effect and topological phase transition in HgTe quantum wells. *Science* 2006;314(5806):1757–61. <https://doi.org/10.1126/science.1133734>.
- [9] Durnev MV, Tarasenko SA. Magnetic field effects on edge and bulk states in topological insulators based on HgTe/CdHgTe quantum wells with strong natural interface inversion asymmetry. *Phys Rev B, Condens Matter* 2016;93. <https://doi.org/10.1103/PhysRevB.93.075434>. 075434.
- [10] Sverdlov V, Selberherr S. Silicon spintronics: Progress and challenges. *Phys Rep* 2015;585:1–40. <https://doi.org/10.1016/j.physrep.2015.05.002>.
- [11] Sverdlov V, Kosina H. Topologically protected and conventional subbands in a 1T'-MoS₂ nanoribbon channel. In: *EUROSIOI-ULIS 2020*; 2020 p. 68–9.
- [12] Sverdlov V, El-Sayed A-M, Kosina H, Selberherr S. Conductance in a nanoribbon of Topologically Insulating MoS₂ in the 1T' phase. *IEEE Trans Electron Devices* 2020; 67(11):4687–90. <https://doi.org/10.1109/TED.1610.1109/TED.2020.3023921>.



Viktor Sverdlov received his Master of Science and PhD degrees in physics from the State University of St.Petersburg, Russia, in 1985 and 1989, respectively. From 1989 to 1999 he worked as a staff research scientist at the V.A.Fock Institute of Physics, St. Petersburg State University. During this time, he visited ICTP (Italy, 1993), the University of Geneva (Switzerland, 1993–1994), the University of Oulu (Finland,1995), the Helsinki University of Technology (Finland, 1996, 1998), the Free University of Berlin (Germany, 1997), and NORDITA (Denmark, 1998). In 1999, he became a staff research scientist at the State University of New York at Stony Brook. He joined the Institute for Microelectronics, *TU Wien*, in 2004. His scientific interests include device simulations, computational physics, solid-state physics, and nanoelectronics.